Journal of
Nanoscience and Nanotechnology
Vol. 8, 907–913, 2008

Particle Morphology of Various SiC-Based Nanocomposite Powders Made by the Aerosol-Assisted Synthesis Method

Cezary Czosnek* and Jerzy F. Janik

AGH University of Science and Technology, Faculty of Fuels and Energy, Al. Mickiewicza 30, 30-059 Kraków, Poland

RESEARCH ARTICLE

Herein, we present a part of a study on the preparation of SiC-based composite nanopowders by the two-stage Aerosol-Assisted Vapor Phase Synthesis (AAVS) method from organosilicon precursors (neat hexamethyldisiloxane, neat tetramethoxysilane, ethanol solutions of polydimethylsiloxane). Upon generation, liquid aerosol droplets were transported in a stream of argon through a ceramic reactor tube maintained at 1200 °C. The resulting solid by-products were collected on a nylon filter as bulk powders. Each raw powder was, subsequently, pyrolyzed in a furnace reactor heated to 1650 °C under a flow of argon. After the final pyrolysis at 1650 °C, mostly nanocrystalline silicon carbide powder with small quantities of free excess carbon was obtained from the neat hexamethyldisiloxane system, composite powder of not fully converted silica and SiC was prepared from the neat tetramethoxysilane system, and C-rich/SiC composite was made from the ethanol/polydimethylsiloxane solution system. The prevailing phase of the SiC component was the regular β-SiC polytype. Most of the powders were composed of spheroidal particles – morphology imprinted during aerosol generation at 1200 °C and not much affected by the second-stage bulk pyrolysis at 1650 °C. The specifics of spheroidal morphology were characteristic of the applied precursor system.

Keywords: Silicon Carbide, Carbon, Composites, Aerosol Synthesis, Morphology.

1. INTRODUCTION

Silicon carbide SiC thanks to its many advantageous properties has found numerous applications in ceramics and electronics. In this regard, often novel, specific properties of nanosized materials forms coupled with their anticipated high utilization potential have resulted in recent years in an intensive research focused on nanocrystalline SiC. For example, in the area of SiC nanopowders, studies have been reported on optical properties of nano-SiC dispersed in photopolymer matrices.[1,2] Similarly, dielectric properties of pure and doped nanopowders of SiC have been investigated at microwave frequencies from 4 to 18 GHz to probe their insulating and electromagnetic wave absorption properties.[3] On the other hand, high thermal and chemical resistance of SiC makes it an advantageous modifying component in various composites and, for instance, in composite systems with carbon C, silicon carbide extends the range of application of such-modified carbon materials, *i.e.*, C/SiC composites.[4,5]

Classical methods for the preparation of SiC include reactions of well mixed/homogenized solid substrates such as elemental Si and C[6] or carbothermal reduction of SiO_2 in the presence of a carbon source such as soot, carbon black, etc.[7] These reactions require relatively high temperatures under which conditions mostly microcrystalline SiC is obtained. In addition, a prerequisite extensive milling/mixing of the solid substrates may introduce a range of contaminants into products. Formation of nanocrystalline SiC was reported in a study utilizing sol–gel chemistry of organosilicon derivatives.[8] Other approach has applied a solution system of sodium silicates (Si-precursors) and sugar (C-precursor).[9] In our contribution, we used heterogeneous mixtures of polycarbomethylsilane, elemental silicon,[10] and polydimethylsiloxane[11] with a coal tar pitch to prepare a range of C/SiC nanocomposites. Conversion temperatures around 1400 °C and higher were required in these precursor systems to produce mainly cubic β-SiC with average crystallite sizes in the range of 14–24 nm.

Another approach to nanocrystalline SiC employs thermally driven decomposition of single-source precursors (compounds containing Si–C moieties). One example of

*Author to whom correspondence should be addressed.

1533-4880/2008/8/907/007 doi:10.1166/jnn.2008.D058

such an idea is the application of polycarbosilane polymers for the preparation of SiC fibers[12, 13] while nanopowder C/SiC composites were also shown to form from the latter precursor in combination with a coal tar pitch.[14] Yet another way to explore this idea is utilization of an aerosol-assisted synthesis method that processes liquid organosilicon precursors and/or their solutions. The aerosol method has already been used with success to prepare nanopowders of BN,[15, 16] GaN,[17, 18] TiN,[19] and GaN-based composites.[20, 21] In the first stage, complex decomposition reactions take place in submicrometer-sized droplets containing precursors (and solvent, if appropriate) during aerosol transport through a high-temperature reactor zone. The as-received aerosol powders obtained from this processing are usually subjected to a second-stage pyrolysis to complete chemical changes of products that have spherical particle morphology. In addition to the latter feature, the main advantages of the aerosol-assisted process are the utilization of affordable precursors and the fact that all reactions take place within very small liquid and solid particles suspended in a reactive gas stream, which creates more-advantageous conditions for nanosized SiC formation compared to typical one-stage bulk solid pyrolysis methods.

A pertinent feature of many thermochemical conversion processes of silicon precursors, particularly, those containing intrinsic oxygen such as molecular and polymeric siloxanes, is a propensity for the formation of glassy silicon oxycarbide SiO_xC_y with variable composition dependent mainly on the type of precursor and, apparently, stable up to 1200 °C.[22, 23] In many cases, in addition to oxycarbide carbon centers, discrete clusters of free carbon also have been postulated to form while being entrapped in the amorphous structure of SiO_xC_y. At higher temperatures of the order of 1400–1600 °C and under neutral gas atmosphere, a separation of phases appears to prevail at the expense of the initial oxycarbide that is manifested by the appearance of nanocrystalline β-SiC, amorphous or crystalline silica SiO_2,[24] and, in certain systems rich in silicon, elemental Si.[25] Similar changes in the copolymer mixtures of silsesquioxanes worked up in the 1200–1400 °C range resulted in mostly amorphous phases of SiO_xC_y, SiC, and SiO_2 accompanied by small amounts of crystalline SiC and turbostratic graphitic carbon.[26] Graphitic carbon formation was also observed after a post-treatment at 1450 °C of the initial oxycarbide derived from the decomposition of polyhydridomethylsiloxane.[27] Interestingly, despite the presence of both forms of carbon, there has been no evidence for efficient carbothermal reduction chemistry that, apparently, loses the competition to phase separation phenomena under the applied conditions of high temperature post-treatment. It is worth pointing out that the reactivity characteristics of the decomposition of siloxanes can be utilized to prepare more complex composite systems of which example is the reaction system of polysiloxanes and Ti-metal.[28]

In this report, are presented preliminary data on nanopowder composites prepared by the two-stage aerosol-assisted synthesis applied to selected oxygen-bearing organosilicon precursor systems. Based mainly on the results of electron scanning microscopy SEM and powder XRD spectroscopy, the evolution of particle size and morphology is discussed for the product powders. It is worth pointing out that these products prepared after the second-stage treatment at 1650 °C, Ar, do not contain any plausible transient oxycarbide species reported to be stable only below 1200 °C.

2. EXPERIMENTAL DETAILS

The aerosol-assisted preparation of raw powders was carried out in an experimental set-up shown schematically in Figure 1.

The reactor tube was made of alumina, 76 mm ID, and 1500 mm in length. The substrates included neat hexamethyldisiloxane, $[(CH_3)_3Si]_2O$ (Aldrich), neat tetramethoxysilane, $Si(OCH_3)_4$ (Aldrich), and ethanol solutions of polydimethylsiloxane, $\{-Si(CH_3)_2-O-\}_n$, $n_{av} = 16$ (Silikony Polskie, Sarzyna, Poland). Note that in the last case, due to the high surface tension of neat polydimethylsiloxane retarding ultrasonic aerosol formation, ethanol solutions of the precursor were used. After generation, an aerosol mist was transported in a stream of Ar gas, 4 L/min, to a pre-heated ceramic reactor tube maintained at 1200 °C. A solid aerosol product was collected on an exit nylon filter. The as-prepared raw products were black free-flowing powders except for the powder from tetramethoxysilane which was brownish black. After examination by analytical methods, the powders were pyrolyzed in the second stage at 1650 °C under a flow of Ar to yield final products. For the purpose of this report, the raw and final products were examined with scanning electron microscopy SEM (Hitachi, Model S-4700), powder XRD spectroscopy (PANanalytical, Model X'Pert Pro, Holland; Cu K_α radiation, $\lambda = 1.54060$ Å), and FT-IR spectroscopy (Nicolet 380, Thermo Electron Corporation). Low temperature oxidation of both raw and final samples was carried out at 700 °C in air for 1.5 hours, and weight losses were recorded that corresponded to excess carbon (free carbon) accessible to reactions with oxygen under

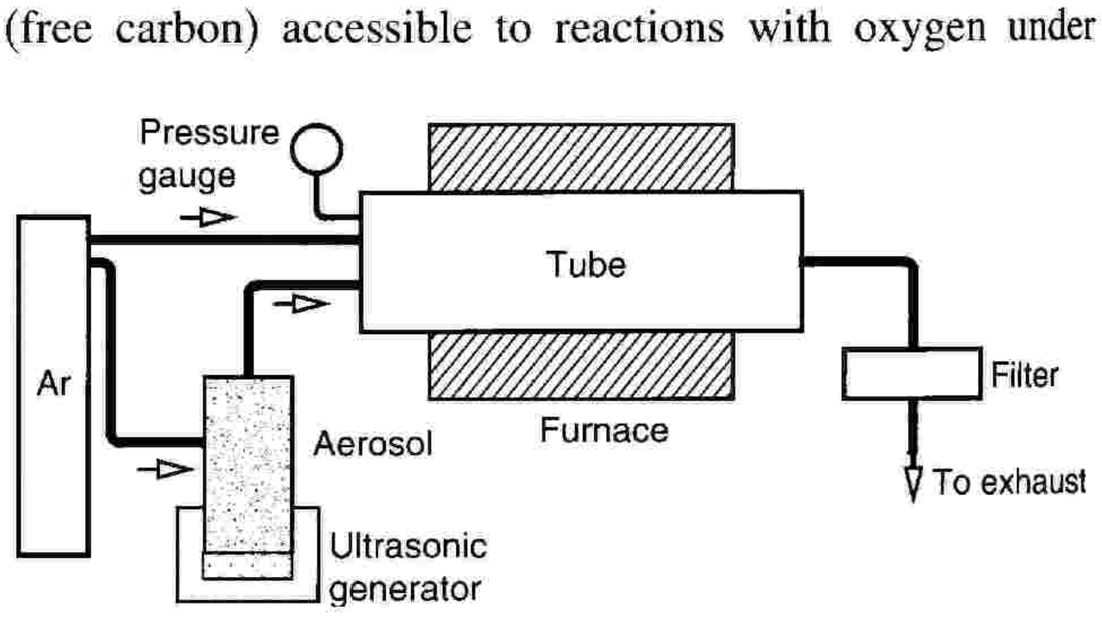

Fig. 1. Overall scheme of the set-up for aerosol powder generation.

applied conditions. Additionally, the carbon content was determined by a standard combustion technique, 1300 °C, in pure oxygen, followed by infrared determination of CO_2 (Model ACS-40/1350 Analyzer, PIE, Warsaw, Poland); this content should in principle correspond to total carbon contents (free carbon plus carbon in SiC) in the composite samples.

3. RESULTS AND DISCUSSION

Figure 2 presents typical SEM micrographs taken for the as-prepared aerosol powders. Especially, in the case of hexamethyldisiloxane (A) and ethanol solutions of polydimethylsiloxane (C), particle morphology is quite typical for the method, *i.e.*, spherical while in many cases the spheres show to be fused together through connecting necks. Spheroidal appearance is displayed also by the as-prepared powder from tetramethoxysilane (B) alas with less distinct features.

In this regard, after an aerosol is generated from a neat precursor (without solvent), the mist of particles is transported by a gas flow through a pre-heated reactor tube and undergoing multistep and complex thermochemical changes of which dynamics impacts the evolution of particle morphology and, therefore, its final appearance. In the first stage, the decomposition primarily affects the outer layers of a droplet resulting in a partially polymerized surface of progressively increased viscosity. The decomposition process of this kind proceeds toward the core of the particle depending on a temperature gradient within a particle. Since the polymerization/condensation of a liquid precursor goes through a viscous stage to the solid state, its overall process dynamics under applied conditions, other things being equal, will decide about the resulting particle morphology, *i.e.*, spherical, spheroidal, and featureless for the relatively fast, intermediate, and slow solidification phenomena, respectively. Complications may arise if during decomposition volatile products are released from the particle's body. The interplay of the effects due to material's viscosity, rates of volatiles formation and solidification can severely deform the particles and in some cases, for example, result in "cauliflower"-type shapes or even empty-shelled spheres. On the other hand, any hindrance to the escape of volatiles such as extremely high viscosities or a lack of porosity in solidified volumes, especially, in surface layers may result in bursting events and production of irregular fines. To add even more to potential complexity of the method, for volatile precursors with high vapor pressure under aerosol generation conditions CVD-like reactions may occur for the vapors in the gas phase to result in formation of the smallest size mode of irregular fines.

A more detailed insight into Figure 2(A) (hexamethyldisiloxane system) shows spherical particles alas of polydisperse sizes mostly in the range of approx. 200–400 nm while in Figure 2(C) (ethanol/polydimethylsiloxane system)

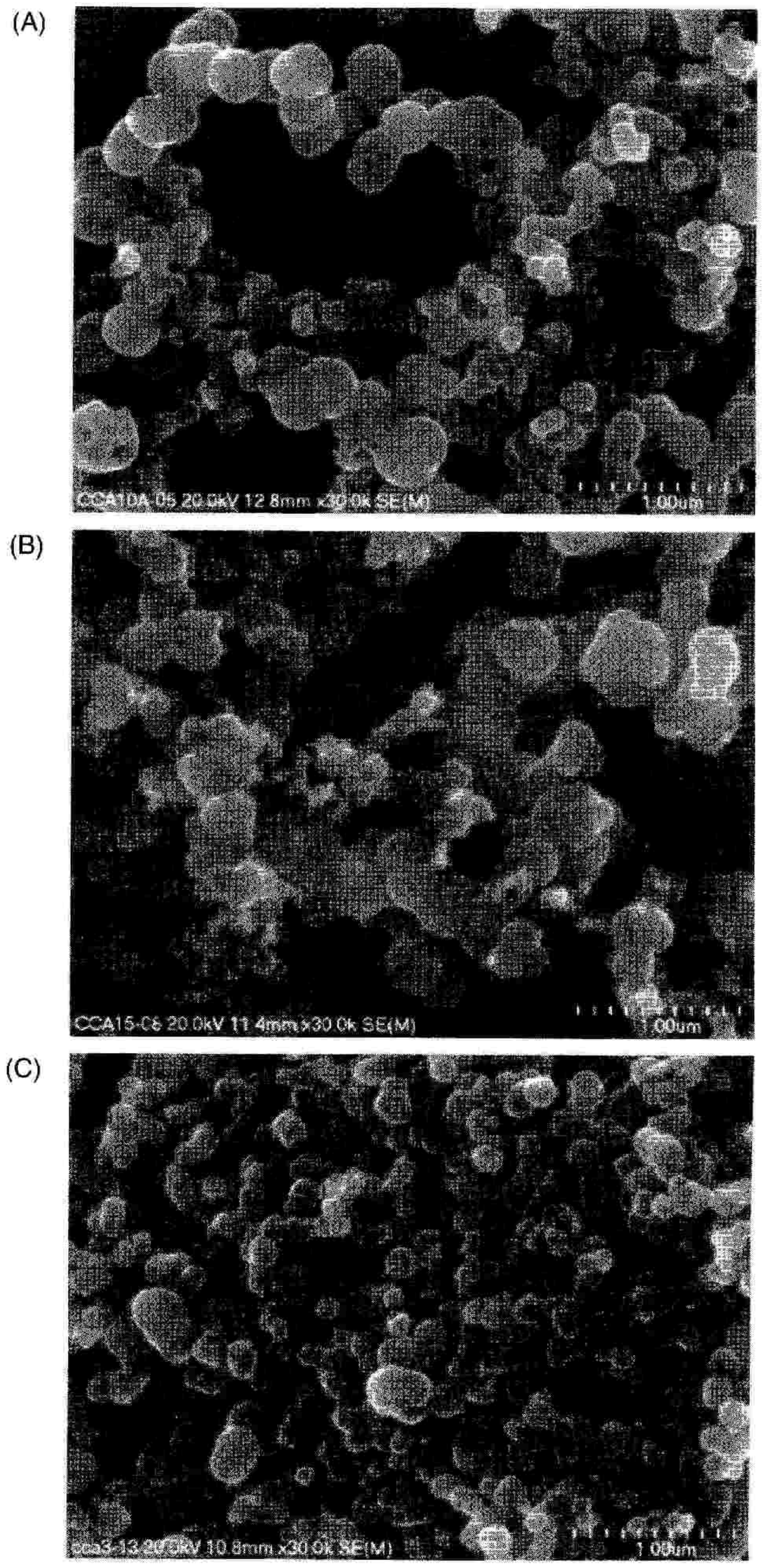

Fig. 2. SEM micrographs of the as-prepared powders obtained at 1200 °C from: neat hexamethyldisiloxane (A), neat tetramethoxysilane (B), solution system ethanol/polydimethylsiloxane (C).

are displayed particles smaller than that, generally, in the range of 100–200 nm. On the other hand, particles from the tetramethoxysilane system displayed in Figure 2(B) appear to be of a bimodal size distribution. First, there are relatively large and bulky aggregates of fused and severely deformed particles but of unquestionable spherical origin based on the rounded outer surfaces. Such aggregates suggest either partial sintering conditions of solid particles[29] or, more likely, in-flight "gluing" among very viscous spheres in no-escape impact events followed by solidifying still in a hot reactor zone before reaching the exit filter. There are also present rather large individual

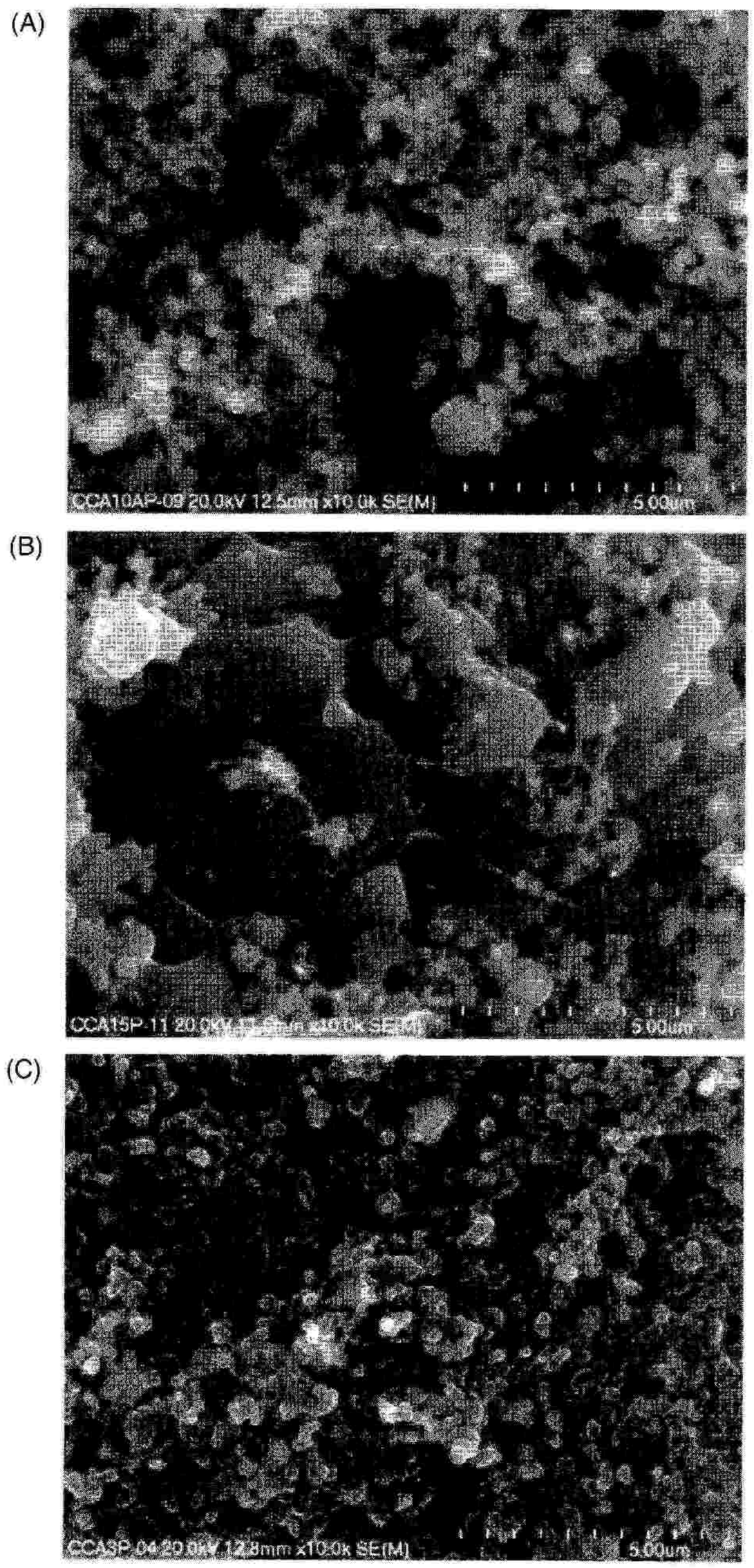

Fig. 3. SEM micrographs of final powders after heat treatment at 1650 °C from: neat hexamethyldisiloxane (A), neat tetramethoxysilane (B), solution system ethanol/polydimethylsiloxane (C).

particles of a spheroidal "cauliflower"-type with sizes in the range of approx. 200–400 nm. Second, there is a distinct fraction composed of fine and irregularly shaped particles much below 200 nm in size. As already mentioned, the latter features indicate reaction circumstances leading to particle bursting upon massive volatiles release and/or accompanying reactions in the vapor phase.

Figure 3 includes the SEM images of the final powders after pyrolysis at 1650 °C under a flow of Ar (note the different magnification bars in Figs. 2 and 3). For the hexamethyldisiloxane and ethanol/polydimethylsiloxane systems, *i.e.*, Figures 3(A) and (C), respectively, the initial particle morphology appears to be preserved both in terms of shape and size. A closer inspection reveals also a number of relatively larger particles with well-developed crystal facelets suggesting an extent of crystal growth/recrystallization phenomena under the pyrolysis conditions; most of the crystallites are, however, confined as nanocrystalline aggregates within the volume of spheroidal particles (*vide infra*). A distinctly different picture emerges from Figure 3(B) (tetramethoxysilane system), namely, in addition to some individual spheroidal particles in the size range encountered in the as-received powder (compare with Fig. 2(B)), there is also an aggregated solid phase of irregular shape implicating a partial melting of one of the components before re-solidification. In fact, one could see with a naked-eye a few very small, colored droplets on the crucible's bottom after powder discharge. As discussed later, the molten component corresponds likely to elemental silicon (m.p. 1410 °C). Another characteristic feature for this powder is its lighter, yellowish-gray color to be compared with grayish-black coloration of the pyrolyzed powders from the other two systems. Additionally, in Figure 3(B) some whisker-type features are found of which growth is usually associated with gas phase reactions. The formation of the volatile oxide Si(II)O from the disproportionation reaction $Si + SiO_2 \rightarrow 2SiO$ and the follow-up reaction involving CO, *i.e.*, $SiO + 3CO \rightarrow SiC + 2CO_2$ would yield silicon carbide whiskers previously observed by us[11] and others[30,31] in related precursor systems.

The SEM/EDX analyses (not shown) of all three final products confirm qualitatively the major conclusions about the chemical nature of different morphological features discussed above. It is especially important to note that in all these cases the distribution of the analyzed elements Si, O, and C is found to be highly homogeneous in various probed areas at micrometer scale proving an advantageous and efficient *in-situ* mixing effect in the precursor-derived composites down to the microsized region.

A detailed account of chemical transformations and product characteristics in these precursor systems will soon be reported elsewhere. However, in order to substantiate relevant morphology aspects, outlined below are the phase composition/crystallite size data derived mainly from powder XRD measurements and low and high temperature oxidation data carried out both for the raw products and 1650 °C-pyrolyzed final products.

Figure 4 shows XRD scans obtained for powders from the neat hexamethyldisiloxane system. The pattern *a* is collected for the as-prepared powder at 1200 °C and shows two broad halos centered at 2 theta equal to approx. 25° and 35°. The pattern is typical for a highly amorphous material; the peak at approx. 25° could correspond to the emergence of turbostratic graphitic domains while the peak at approx. 35° could be traced to emerging β-SiC nanocrystallites.[10] We note that plausible transient amorphous phases of the type SiO_xC_y are not expected to be

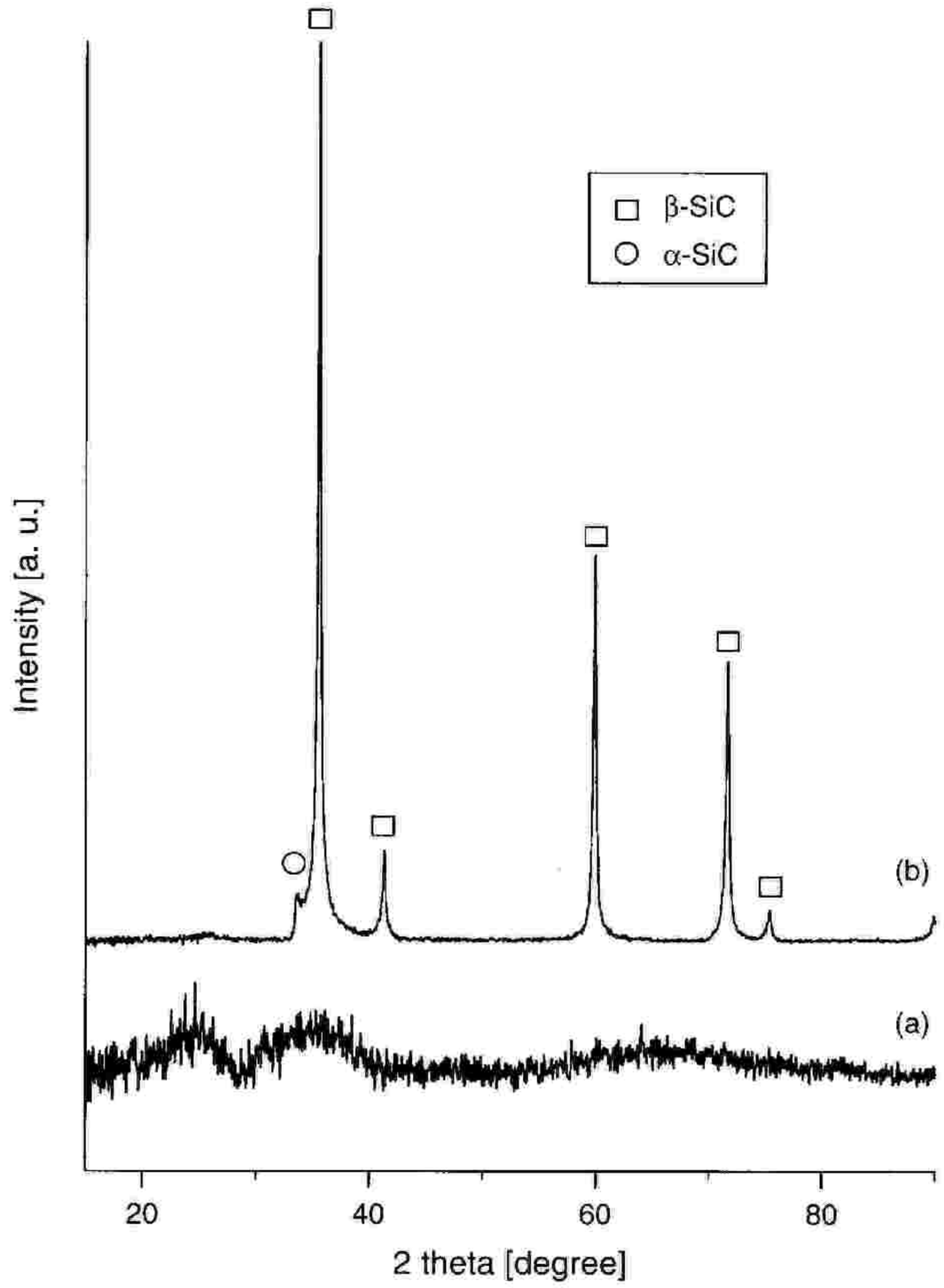

Fig. 4. XRD patterns of powders obtained from neat hexamethyldisiloxane; (a) as-prepared at 1200 °C, (b) after heat treatment at 1650 °C, Ar.

detected by this method. In this regard, infrared spectra for the aerosol powder (not shown) suggest the presence of such species by confirming Si–O bonds. The upper pattern *b* is obtained for the product pyrolyzed at 1650 °C under an argon flow. The most intense set of the relatively sharp peaks is attributed to the regular phase of nanosized β-SiC with an average crystallite size calculated from Scherrer equation of approx. 32 nm. There is also a minor phase of hexagonal α-SiC. Interestingly, no clear evidence can be drawn from the pattern about the occurrence of a plausible phase of turbostratic graphitic carbon. The latter could be expected based on pattern *a* suggesting an excess of carbon in the as-prepared product at 1200 °C. In this regard, the low temperature oxidation of this material yielded 9.5 wt% of excess carbon consistent with the XRD data. However, carbothermal reduction reactions involving the partially carbided SiO_xC_y species that take place at 1650 °C would have resulted in consumption of this small surplus carbon, at least down to detection limits of the XRD method. This is supported by the low temperature oxidation results for the final product showing 7.7 wt% excess carbon. On the other hand, total carbon determination for this product gave 33.7 wt% C to be favorably compared with the value of 35.4 wt% C calculated for the composite system of 92.3 wt% SiC + 7.7 wt% C, the latter derived from the low temperature oxidation data. It is useful to be reminded that any severe deficiency of carbon in the system *versus* the quantity necessary for the reduction of Si–O moieties would have yielded also a crystalline SiO_2 by-product. Therefore, it appears that the 1650 °C-product from the system is mainly the nanocrystalline silicon carbide β-SiC containing small quantities of excess free carbon.

Figure 5 shows the XRD scans collected for materials in the neat tetramethoxysilane system, *i.e.*, pattern *a* for the as-prepared aerosol powder at 1200 °C and pattern *b* for the product pyrolyzed at 1650 °C under argon. In the former, the very broad halo centered at approx. 20–22° is consistent with highly amorphous silica formed from decomposition of the precursor during aerosol generation. The 1650 °C-pyrolyzed material shows the presence of the prevailing nanocrystalline β-SiC, minor quantities of α-SiC, and some crystobalite SiO_2. It is worth noticing that the average crystallite size of β-SiC is approx. 9 nm much less than 32 nm found for the similar product from the previously discussed hexamethyldisiloxane system. We also note that the sample used here for the XRD determination was deprived of a very small quantity of a molten component, *i.e.*, a couple of small spheres found on the crucible's bottom. The component is likely to be molten silicon (m.p. 1410 °C). This fact coupled with the presence of SiO_2 points out to insufficient carbon in the system that otherwise acts towards silica as a reducing agent to yield SiC. Consistent with this is the negligible excess carbon

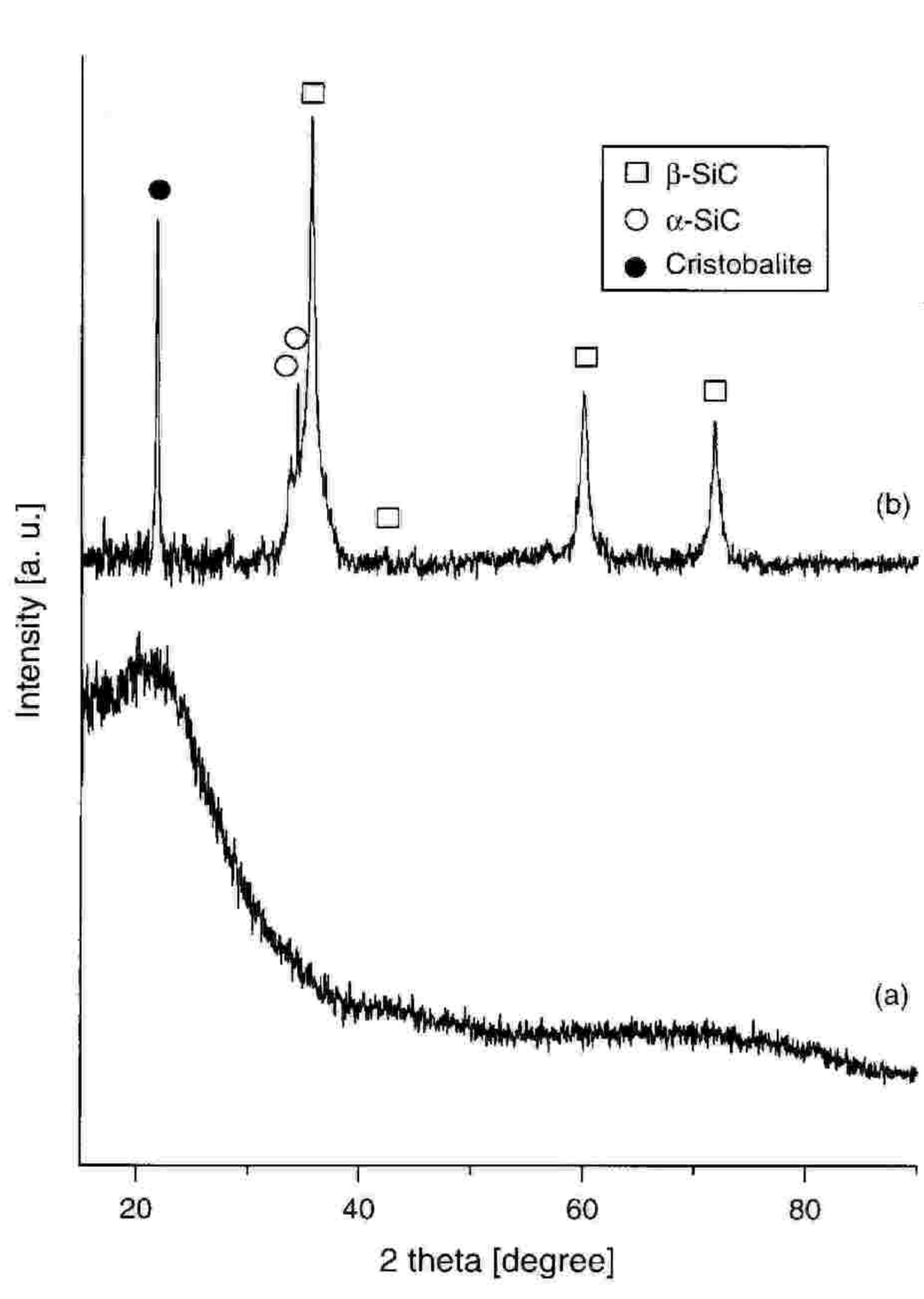

Fig. 5. XRD patterns of powders obtained from neat tetramethoxysilane; (a) as-prepared at 1200 °C, (b) after heat treatment at 1650 °C, Ar.

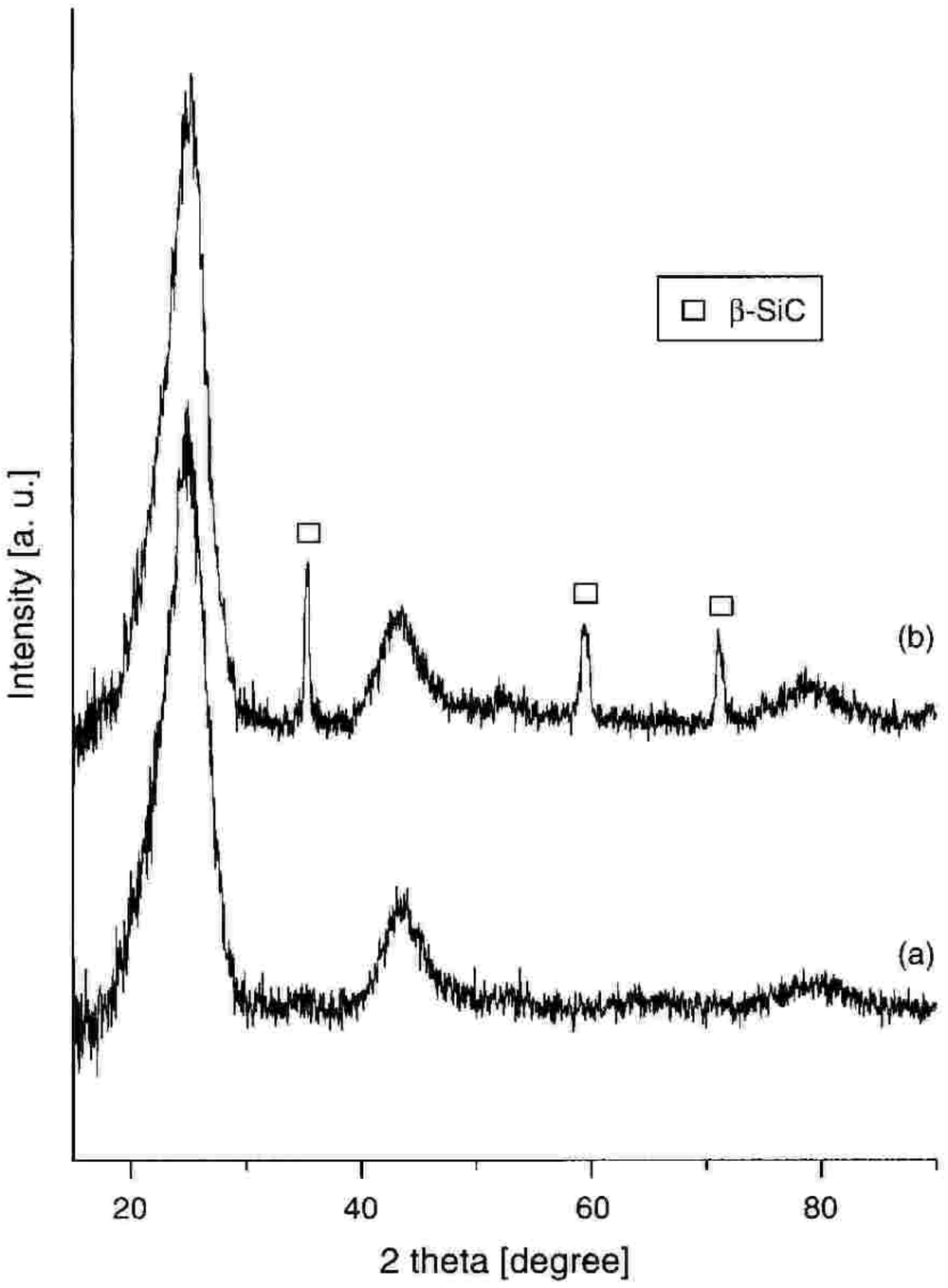

Fig. 6. XRD patterns of powders obtained from the solution system ethanol/polydimethylsiloxane; (a) as-prepared at 1200 °C, (b) after heat treatment at 1650 °C, Ar.

derived from low temperature oxidation (<1 wt%) and total carbon content of 7.2 wt% in the 1650 °C-pyrolyzed material ($SiC + SiO_2$).

Figure 6 displays XRD scans for materials made in the solution system ethanol/polydimethylsiloxane. Spectrum *a* collected for the as-prepared aerosol powder at 1200 °C is characteristic of the broad peaks at 2-theta of approx. 25, 43, and 80° that are associated with turbostratic graphitic domains. No other lines/peaks are seen in this spectrum indicating a highly amorphous nature of any inorganic intermediate phase(s) present in this temperature range. These observations are consistent with abundance of carbon in the system from thermal cracking of ethanol. A good illustration of the 1200 °C-material's composition is the excess carbon of 85.5 wt% and total carbon of 94.9 wt%. Spectrum *b* was obtained for the 1650 °C-pyrolyzed product in this system. It features the broad peaks due to turbostratic graphite that are almost of the same fundamental characteristics as discussed earlier for the as-prepared aerosol powder. Additionally, somewhat broadened peaks typical for β-SiC are seen supporting efficient carbide formation under the condition of excess carbon in the system. The calculated average crystallite size of β-SiC is 9 nm similarly as found in the neat tetramethoxysilane system. The inhibiting effect of the *in-situ* formed nanocrystalline SiC on graphitic domain growth/crystallization in the C-matrix in this temperature range was also observed by us in other precursor systems leading to C/SiC nanocomposites.[10] The excess carbon for this material of 73.5 wt% and the total carbon content of 94.5 wt% in comparison with the similar data for the raw 1200 °C-material appear to indicate the efficiency of carbothermal reduction after the high temperature treatment in this system.

To conclude this section, the picture that emerges from the discussed SEM, XRD, and analytical data for the final products supports the persistence of an overall spheroidal morphology of composite particles, a feature of the applied aerosol synthesis method. It is obvious that phase separation/recrystallization phenomena and accompanying carbothermal reduction chemistry taking place in the various products at 1650 °C cause relatively minor alas specific changes in morphology *versus* the appearance of the initial aerosol-generated products. These changes depend on the particular precursor system. For example, for neat hexamethyldisiloxane in which due to the apparently advantageous proportion of C/Si/O silicon carbide was prevailingly synthesized, an evolution of relatively larger crystallites of SiC is evident in addition to the bulk of spheroidal particles the latter composed of nanosized SiC. In the system of neat tetramethoxysilane with an abundance of intrinsic oxygen, the amount of available carbon needed for an efficient reduction towards SiC is too small and the $SiC + SiO_2$ composite is formed; this has important implications for the product morphology since the silica particles partially melt to form irregularly shaped secondary features. Finally, in the solution system of ethanol/polydimethylsiloxane characterized by large excess of carbon, an overall spheroidal particle morphology of the C/SiC composite is retained while recrystallization of silicon carbide results in the appearance of some regularly shaped SiC crystallites still in the low nanosized region.

4. CONCLUSIONS

The convenient two-stage aerosol-assisted synthesis method showed its utility for the preparation of a range of SiC-based nanomaterials from various single-source and solution precursor systems. After final pyrolysis at 1650 °C under argon, mostly nanocrystalline silicon carbide powder was obtained from the neat hexamethyldisiloxane system, composite powder of not fully converted SiO_2 and SiC was prepared from the neat tetramethoxysilane system, and C-rich/SiC composite was made from the ethanol/polydimethylsiloxane solution system. The prevailing phase of SiC was in all cases the regular β-SiC polytype with the average crystallite size in the 9–32 nm range. The component particles of the composites were homogeneously distributed throughout the bulk of powders. Most of the powders were composed of spheroidal particles – morphology imprinted during aerosol generation at 1200 °C and only slightly affected by the second-stage bulk pyrolysis at 1650 °C under argon. In general,

the utilization of the different Si–O-bearing precursor systems resulted not only in various powder compositions but yielded differing morphologies with overall spheroidal characteristics. Finally, the aerosol-assisted synthesis method appeared to minimize the consequences of the formation of transient oxycarbide species in these precursor systems while creating advantageous conditions for carbothermal reduction towards various SiC-based composite powders.

Acknowledgment: We want to acknowledge support of the Ministry of Science and Higher Education (Poland), Grant No. 3 T08D 035 30.

References and Notes

1. A. Kassiba, M. Tabellout, S. Charpentier, N. Herlin, and J. R. Emery, *Solid State Commun.* 115, 389 (**2000**).
2. I. V. Kityk, M. Makowska-Janusik, A. Kassiba, and K. J. Plucinski, *Opt. Mater.* 13, 449 (**2000**).
3. J. Sun, J. Li, G. Sun, B. Zhang, S. Zhang, and H. Zhai, *Ceram. Int.* 28, 741 (**2002**).
4. X. Yin, L. Cheng, L. Zhang, and Y. Xu, *Carbon* 40, 905 (**2002**).
5. L. Cheng, Y. Xu, L. Zhang, and X. Luan, *Carbon* 40, 2229 (**2002**).
6. L. N. Satapathy, P. D. Ramesh, D. Agrawal, and R. Roy, *Mater. Res. Bull.* 40, 1871 (**2005**).
7. R. Koc and S. V. Cattamanchi, *J. Mater. Sci.* 33, 2537 (**1998**).
8. H.-P. Martin, R. Ecke, and E. Muller, *J. Eur. Ceram. Soc.* 18, 1737 (**1998**).
9. S. Pan, Y. Yang, J. Zhang, and G. Song, *J. Mater. Sci.* 40, 4679 (**2005**).
10. C. Czosnek, W. Ratuszek, J. F. Janik, and Z. Olejniczak, *Fuel Proc. Technol.* 79, 199 (**2002**).
11. C. Czosnek, J. Wolszczak, M. Drygaś, M. Góra, and J. F. Janik, *J. Phys. Chem. Solids* 65, 647 (**2004**).
12. S. Yajima, *Am. Ceram. Soc. Bull.* 62, 893 (**1983**).
13. S. Yajima, Y. Hasegawa, J. Hayashi, and M. Iimura, *J. Mater. Sci.* 13, 2569 (**1978**).
14. C. Czosnek, J. F. Janik, and Z. Olejniczak, *J. Cluster Sci.* 13, 487 (**2002**).
15. E. A. Pruss, G. L. Wood, W. J. Kroenke, and R. T. Paine, *Chem. Mater.* 12, 19 (**2000**).
16. R. T. Paine, W. J. Kroenke, E. A. Pruss, G. L. Wood, and J. F. Janik, U.S. Patent 6 824 753, (**2004**).
17. G. L. Wood, E. A. Pruss, and R. T. Paine, *Chem. Mater.* 13, 12 (**2001**).
18. J. F. Janik, M. Drygaś, S. Stelmakh, E. Grzanka, and B. Pałosz, R. T. Paine, *Phys. Status Solidi A* 203, 1301 (**2006**).
19. M. Drygaś, C. Czosnek, R. T. Paine, and J. F. Janik, *Chem. Mater.* 18, 3122 (**2006**).
20. J. F. Janik, M. Drygaś, C. Czosnek, M. Kamińska, M. Palczewska, and R. T. Paine, *J. Phys. Chem. Solids* 65, 639 (**2004**).
21. M. Drygaś, C. Czosnek, R. T. Paine, and J. F. Janik, *Mater. Res. Bull.* 40, 1136 (**2005**).
22. J. Parmentier, G. D. Sorarù, and F. Babonneau, *J. Eur. Ceram. Soc.* 21, 817 (**2001**).
23. G. D. Sorarù and D. Suttor, *J. Sol-Gel Sci. Technol.* 14, 69 (**1999**).
24. H. Brequel, J. Parmentier, G. D. Sorar, L. Schiffini, and S. Enzo, *Nanostruct. Mater.* 11, 721 (**1999**).
25. G. Gregori, H.-J. Kleebe, D. W. Readey, and G. D. Sorarù, *J. Am. Ceram. Soc.* 89, 1699 (**2006**).
26. F. I. Hurwitz, P. Heimann, and S. C. Farmer, *J. Mater. Sci.* 28, 6622 (**1993**).
27. Y. D. Blum, D. B. MacQueen, and H.-J. Kleebe, *J. Eur. Ceram. Soc.* 25, 143 (**2005**).
28. H. Deniz Akkaş, M. Lütfi Öveçoğlu, and Metin Tanoğlu, *J. Eur. Ceram. Soc.* 26, 3441 (**2006**).
29. F. E. Kruis, K. Kusters, S. E. Pratsinis, and B. Scarlett, *Aerosol Sci. Technol.* 19, 514 (**1993**).
30. B. Kumar and M. M. Godkhindi, *J. Mater. Sci. Lett.* 15, 403 (**1996**).
31. Y.-J. Lin and C.-P. Tsang, *Ceram. Int.* 29, 69 (**2003**).

Received: 20 June 2006. Revised/Accepted: 4 December 2006.